



Enhancement of the O₂ Sensitivity: ZnO, CuO, and ZnO/CuO Hybrid Additives' Effect on Meso-Tetraphenylporphyrin Dye

Merve Zeyrek Ongun^{1*}

¹Dokuz Eylul University, Chemistry Technology Program, Izmir, 35360, Turkey

Abstract: Semiconductor metal oxide materials have attracted great interest in gas sensors due to their high sensitivity to many target gases. In this study, an oxygen-sensitive optical chemical sensor was prepared in thin-film form by immobilizing meso-tetraphenylporphyrin (H₂TPP) in silicon matrix in the presence of ZnO, CuO and ZnO/CuO hybrid nanoparticles as additives. Characterization of synthesized metal oxide powders was performed using XPS, XRD, SEM, and PL spectroscopy. Emission and decay time measurements of H₂TPP-based materials were investigated between the concentration range of 0% and 100% [O₂] in thin-film forms. The intensity-based signal drops of the additive-free form of porphyrin dye toward oxygen were calculated as 70%. Whereas, the oxygen sensitivities of H₂TPP-based sensor slides were measured as 80%, 75%, and 88% in the presence of ZnO, CuO, and ZnO/CuO hybrid particles, respectively. The usage of porphyrin dye with ZnO/CuO hybrid additive provided higher oxygen sensitivity, larger linear response range, higher Stern-Volmer constant (KSV) value and faster response time compared to the undoped form, ZnO and CuO additive-doped forms of H₂TPP. The response and the recovery times of the porphyrin-based sensing slide along with ZnO/CuO hybrid particles have been measured as 10 and 20 s. These results make the H₂TPP along with the metal oxide additives promising candidates as oxygen probes.

Keywords: Photoluminescence, oxygen sensor, H₂TPP, ZnO, CuO, ZnO/CuO hybrid.

Submitted: December 02, 2021. **Accepted:** March 10, 2022.

Cite this: Zeyrek Ongun M. Enhancement of the O₂ Sensitivity: ZnO, CuO, and ZnO/CuO Hybrid Additives' Effect on Meso-Tetraphenylporphyrin Dye. JOTCSA. 2022;9(2):479-94.

DOI: <https://doi.org/10.18596/jotcsa.1031613>.

***Corresponding author. E-mail:** merve.zeyrek@deu.edu.tr. Telephone number: 05309372673.

INTRODUCTION

Oxygen is used as a reactant or product (1) in industrial processes, clinical (2), biomedical (3), environmental (4), and chemical analysis (5), and therefore, continuous and accurate determination of dissolved and gaseous O₂ levels is of great importance. In recent decades, optical chemical sensors based on spectroscopic changes are currently preferred for oxygen detection due to many advantages such as easy fabrication, high sensitivity, low detection limit, and low cost. Most optical sensors are fabricated by doping different types of oxygen-sensitive organic dyes into gas permeable sol-gel or polymeric matrices. There are

different types of organic dyes such as transition metal complexes of ruthenium (2), iridium (6), palladium (7), platinum (8), osmium (9), pyrene (10), and porphyrin and derivatives (11) used as oxygen-induced optical sensors based on the working principle of luminescence-quenching. One of the most important phosphorescence dyes used in oxygen gas sensors is metal-free and metal-carrier forms of tetraphenylporphyrins (TPPs), because of their long fluorescence lifetimes (microsecond to millisecond range), high oxygen sensitivity, large Stokes' shifts, high quantum yields, fast response times, and long stabilities. Table 1 summarizes previous studies with different porphyrin derivatives (12-20).

Table 1: Comparison of the oxygen sensing properties of porphyrin derivatives.

Sensitive dye	Matrix material	Sensitivity	Dynamic working range	Detection limit	Response time (N2-O2 / O2-N2)	Stability	Ref.
PdTPA PtTPA PdTPP PtTPP	poly(TMSP)	Ksv (% ⁻¹) 3.05 2.48 0.47 0.63	0-100% pO ₂	0.00098 0.012 0.0062 0.0047	6; 5; 13; 6 / 117; 46 s	After 8 months 20% lost	(12)
PdTFPP PdTCPP	Sol-gel	I ₀ /I ₁₀₀ 21.7 7.4	0-40 mg/L	NR	NR / NR	NR	(13)
PdTFPP	Silica-gel	KSV 67 kPa ⁻¹	0.02-100 Pa	NR	150ms / NR	NR	(14)
PdTPP	PMMA	KSV 0.071 Torr ⁻¹	0-200 Torr ⁻¹	NR	NR / NR	After 9 months 75% lost	(15)
PdTPTBP	Silicone rubber	KSV 0.921 hPa ⁻¹	213 hPa to 0 hPa O ₂	NR	<1s / NR	NR	(16)
PtTFPP	PS	KSV (% ⁻¹) 0.018	0-100% pO ₂	NR	NR / NR	NR	(17)
H ₂ TPP H ₂ TPA H ₂ OHe	poly(TMSP)	I ₀ /I ₁₀₀ 1.46 2.85 2.16	0-100% pO ₂	NR	NR / NR	After 3 months 6% lost	(18)
ZnTPP H ₂ TPP	poly(TMSP)	KSV (% ⁻¹) 0.0052 0.0384	0-20% pO ₂	NR	2 / 3 s	After 5 months 2% lost	(19)
H ₂ TPP	plastic-clad silica optic fiber	KSV = 7.5 × 10 ⁻⁴ Torr ⁻¹ I ₀ / I ₁₀₀ ≈ 1.55	55-760 Torr ⁻¹	NR	1s / NR	NR	(20)
H ₂ TPP H ₂ TPP-ZnO H ₂ TPP-CuO H ₂ TPP-ZnO/CuO Hybrid	poly(TMSP)	I ₀ /I ₁₀₀ 3.39 6.02 4.88 7.35	0-100% pO ₂	1.25 × 10 ⁻² 2.21 × 10 ⁻² 1.89 × 10 ⁻² 2.84 × 10 ⁻²	16; 12; 14; 10 s / 34; 24; 28; 20 s	After 6 months 3% lost	This work

NR= Not Reported

The sensing properties of fluorescent dyes depend on the interactions between the kind of solid matrix and the type of micro-environment of dyes. The appropriate polymer matrix can play a role as an enhancer agent in the oxygen sensitivity properties and provide mechanical stability due to being a rigid support material. However, the polymer-immobilized organic dyes still need some further modifications to improve their oxygen sensing performances. To increase the oxygen sensitivity of organic dyes, different ligand groups are attached to the structure of the dye, which can interact with oxygen groups during dye synthesis, or different semiconducting metal oxides known to have oxygen

adsorption abilities are added to the dye as a dopant during the preparation of the chemical sensor.

Semiconducting metal oxides (SMO) are promising candidate materials for gas sensing applications due to their easy production methods, high sensitivity to many target gases, low cost and being highly compatible with other processes (21). According to the literature, many gas sensor studies containing metal oxide nanoparticles due to porous structure and change of conductivity properties are based on electrical measurement. Recently, the use of many metal oxide nanoparticles such as ZnO, CuO, NiO₂,

TiO₂, etc. has become a new and popular application to improve electronic tape structure and enhance gas detection performance. Wang et al. reported that the CO gas detection capability of CuO/ZnO composite nanostructure was measured by the relative resistance techniques (22). Jiang et al. found that the fabricated ure and Pr-modified ZnO nanofibers synthesized using electrospinning-calcination techniques showed intensity-based O₂ sensing responses as 52% and 71%, at 115 °C, respectively (23). Inspired by these studies, today researchers include metal oxides with gas adsorption properties in optical chemical sensor studies. The advantage of fluorescence-based measurement is to be seen as an alternative in the absence of electrical contact between the resulting impurities and nanostructures. Last decades, many approaches were used such as adding some dopants like metals (Au (24), Ag (25), etc.) and/or metal oxides (SnO₂ (26), ZnO (27), TiO₂ (28), CuO (29) and Fe₂O₃ (30), etc.) because of their gas adsorption properties. Mariammal and colleagues reported that ZnO and ZnO:CuO nanoparticle-based sensing composites were used to detect ethanol vapor using the fiber optic sensor method (31). The emission and excitation spectra of transparent nanocolumnar porous ZnO thin films prepared by plasma-enhanced chemical vapor deposition were measured in the presence and absence of dissolved oxygen by Sanchez-Valencia et al. (32). Nowadays, researchers work on the enhancement of the gas sensitivity properties of organic dyes by supplementing additives such as metal and/or metal oxides. Jiang and co-workers fabricated a ratiometric optical sensor for dissolved oxygen in a form of nanofiber and thin-film using together Ag NPs and (Ru(dpp)₃Cl₂) composite via immobilized in polymethylmethacrylate matrix (33). Ozturk et al. investigated the effect of Ag NPs and ionic liquids (1-butyl-3-methylimidazolium tetrafluoroborate) on oxygen sensitivity of the ruthenium (II) dye in a form of fiber materials and nanoporous film structures (34). Ongun developed a high sensitive oxygen-induced sensor including the meso-tetraphenylporphyrin (H₂TPP) dye encapsulated in a silicon matrix in the presence of additives as Ag NPs and ionic liquids (ILs) (35). Oguzlar reported that the Fe₃O₄ and Fe₃O₄@Ag NPs as additives were used for improving oxygen sensing properties of the [Ru(bpy)₃]²⁺ dye both in EC thin-film and nanofiber form (36).

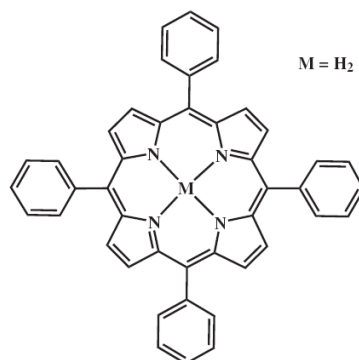
In this study, we aimed to improve the oxygen-induced sensitivity of commercially available meso-tetraphenylporphyrin (H₂TPP) dye in the presence of

different metal oxide additives. While both ZnO and CuO particles were produced by the sol-gel method, ZnO/CuO hybrid nanoparticles were synthesized using the complex directed hybridization method. The synthesized particles were characterized using photoluminescence spectroscopy (PL), X-ray photoelectron spectroscopy (XPS), X-ray diffraction spectroscopy (XRD), and scanning electron microscopy (SEM). The oxygen sensing responses of the H₂TPP-based composites along with metal oxide additives embedded in the poly(1-trimethylsilyl-1-propyne) matrix were tested by measuring the fluorescence-based emission spectra and decay time measurements. The relative signal intensity (I_0/I_{100}) values of H₂TPP along with the ZnO, CuO, and ZnO/CuO hybrid additives were found as 6.02, 4.88, and 7.35 between the concentration range of 0 and 100% [O₂], respectively. The enhancement of the emission-based optical properties and the decay kinetics can be based on the adherence of the oxygen molecules to the surface or inside of the metal oxide crystalline structures via adsorption. The usage of the ZnO, CuO and ZnO/CuO hybrid particles along with the H₂TPP resulted in higher oxygen sensitivity, faster response, more linear calibration plots, and better sensor dynamics compared to the non-additive free-form of dye.

EXPERIMENTAL SECTION

Reagents

Precursors were used without further purification in the synthesis of metal oxide nanoparticles. Zinc acetate dihydrate (Zn(CH₃COO)₂×2H₂O, ≥99%), zinc nitrate heptahydrate (Zn(NO₃)₂×7H₂O, ≥99%), and copper(II) acetate dihydrate (Cu(CH₃COO)₂×2H₂O, ≥99%) were purchased from Sigma Aldrich. Oxygen sensitive fluorescent dye, free-form of meso-tetraphenylporphyrin (H₂TPP), was supplied from Sigma-Aldrich. The structural formula of the employed metal-free porphyrin dye was shown in Scheme 1. Poly(1-trimethylsilyl-1-propyne) (poly(TMSP)) as polymeric support material was provided by ABCR Company. 1-Butyl-3-methylimidazolium tetrafluoroborate [BMIM][BF₄], used as an ionic liquid (IL), was obtained from Fluka. Sodium hydroxide (NaOH, ≥99%) was from Alfa-Aesar Sigma-Aldrich. The solvents of ethanolamine (≥98%) and toluene (≥99%) were purchased from Sigma-Aldrich. Mylar, polyester support for thin-film preparation, was supplied from DuPont polymers. Cylinders of nitrogen and oxygen gases (99.99%) were provided from Tinsa Gas, Izmir, Turkey.



Scheme 1: Structural formula of the metal-free tetraphenylporphyrin (H_2TPP).

Instrumentation

The phase structure of the synthesized powders was investigated by an X-ray diffractometer (XRD, Thermo Scientific ARL X-ray diffractometer, Cu-K α , 1.5405 Å, 45kV, 44mA). Thermo Scientific K-Alpha X-ray Photoelectron Spectrometer (XPS) equipped monochromatic Al-K α source was used to determine the elemental compositions of metal oxide particles. For morphological characterization, microstructure images were studied at different magnifications by COXEM EM-30 Plus scanning electron microscopy (SEM). The excitation-emission spectra were measured via Edinburgh FLSP920 spectrometer (PL). Decay time measurements under the excitation of a microsecond flash lamp were determined by the photoluminescence spectrometer operating on the time-dependent single-photon count (TCSPC) principle. Oxygen and nitrogen gases were mixed between 0% and 100% [O_2] concentration range using a gas blending system (Sonimix 7000A) and the gas mixture was introduced to the sensing thin film membrane in septum-sealed cuvette at room temperature via a diffuser needle.

Syntheses of ZnO, CuO and ZnO/CuO Hybrid Particles

The ZnO and CuO particles were synthesized by the sol-gel method. For the production of ZnO NPs, 0.5 M Zn(NO $_3$) $_2$ ·7H $_2$ O solution was added dropwise into the 1 M NaOH solution and heated at 70 °C for 2 h. The obtained white precipitates were dried at 200 °C for 1 h and then calcinated at 500 °C for 2 h (25). Similarly, in the preparation of CuO NPs, Cu(CH $_3$ COO) $_2$ ·2H $_2$ O powder (0.5 M) was dissolved in isopropanol, stirred and heated for 1 h at 50 °C. The pH value of the copper solution was adjusted using ethanolamine. The black precipitates were dried at 100 °C for 5 h and calcinated at 600 °C for 2 h, respectively (37). To prepare the ZnO/CuO hybrid NPs were used the complex directed hybridization method; 0.5 M Zn(CH $_3$ COO) $_2$ ·2H $_2$ O and 0.5 M Cu(CH $_3$ COO) $_2$ ·2H $_2$ O solutions were dissolved separately in distilled water and then mixed. While 10 M NaOH solution was added dropwise, the solution was stirred with a magnetic

stirrer. The final solution was heated for 12 h at 100 °C, then the calcination process was applied for 3 h at 500 °C (38).

Preparation of H $_2$ TPP-based oxygen sensing slides

Nowadays, researchers work on the enhancement of O $_2$ -sensing characteristics of porphyrin dyes along with different kinds of additives embedded in several polymeric matrices. The fluorescent-based sensing abilities of gas sensors are severely connected to the type of solid matrix and possible additive. In our previous works, we found that poly(TMSP) is an ideal polymeric matrix according to the optical transparency, high diffusibility toward oxygen, and stability. Therefore, poly(TMSP) was selected as a polymeric support material due to the high polymer permeability (oxygen permeability coefficient ($L = 7700 \text{ cm}^3 \text{ (STP) cm/cm}^2 \cdot \text{s} \cdot \text{cm Hg}$) and rapidly in contact with molecular oxygen (11,18). Also, we found in our previous work that the best ionic liquid additive is the [BMIM][BF $_4$] in terms of compatibility and oxygen gas solubility in a polymeric matrix and providing long-term stability to the indicator dye doped-sensing slides (39). Considering this information, thin films were prepared by placing meso-tetraphenylporphyrin (H_2TPP) dye embedded in poly(TMSP) matrix along with both different metal oxide additives and ionic liquid in close proximity.

The homogenous sensing slides were prepared by mixing 75 mg of poly(TMSP), 0.25 mg porphyrin dye, and 25 mg of [BMIM][BF $_4$] in 2.5 mL toluene under magnetic stirring. To improve the oxygen sensitivity of the H_2TPP dye, 0.25 mg of metal oxide (ZnO, CuO and ZnO/CuO hybrid) particles were individually added to the cocktail solution. Table 2 presents the compositions of the utilized cocktails. Afterwards, the prepared viscous solutions were coated onto a Mylar support using the knife spread method. Tencor Alpha Step 500 Profilometer was used to measure the thickness of the coated thin films ($7.63 \pm 0.18 \mu\text{m}$ ($n = 8$)). The measurements were recorded after each thin film was cut to appropriate sizes and placed in the septum cuvette.

Table 2: Cocktail compositions used as oxygen-sensing agents.

Dye	Cocktail Name	poly(TMSP) (mg)	toluene (mL)	ILs (mg)	Additive/ ZnO (mg)	Additive/ CuO (mg)	Additive/ ZnO/CuO Hybrid (mg)
H ₂ TPP (0.5 mg)	C1	75	2.5	25	-	-	-
	C2	75	2.5	25	0.5	-	-
	C3	75	2.5	25	-	0.5	-
	C4	75	2.5	25	-	-	0.5

RESULTS AND DISCUSSION

Characterization of metal oxide particles

The structural changes of the produced particles were examined by XRD (Figure 1 (a)). XRD peaks of the ZnO [JCPDS No. 36-1451] at $2\theta = 31.8^\circ, 34.5^\circ, 47.5^\circ, 56.5^\circ, 62.9^\circ, 66.4^\circ, 67.9^\circ, 69.2^\circ, 72.6^\circ$ and 77.0° were observed, consist with (100), (002), (101), (102), (110), (103), (112), (004) and (202) crystallographic planes of the ZnO hexagonal wurtzite phase, respectively (40). The diffraction peaks of the CuO [JCPDS No. 48-1548] at $2\theta =$

$32.6^\circ, 35.7^\circ, 38.9^\circ, 49.0^\circ, 53.6^\circ, 61.7^\circ, 66.2^\circ, 68.4^\circ, 66.2^\circ, 68.4^\circ$ corresponding to (110), (002), (111), (202), (020), (202), (113), (022), (220), (312), and (203) crystallographic planes of the CuO, which indicates that the CuO is monoclinic (41). Additionally, the diffraction peaks of the ZnO/CuO hybrid (1:1 molar ratio) nanocomposite were well matched with the above JCPDS cards, and the XRD patterns can be easily indexed to a mixed crystal phase containing a hexagonal wurtzite ZnO phase and a monoclinic (38).

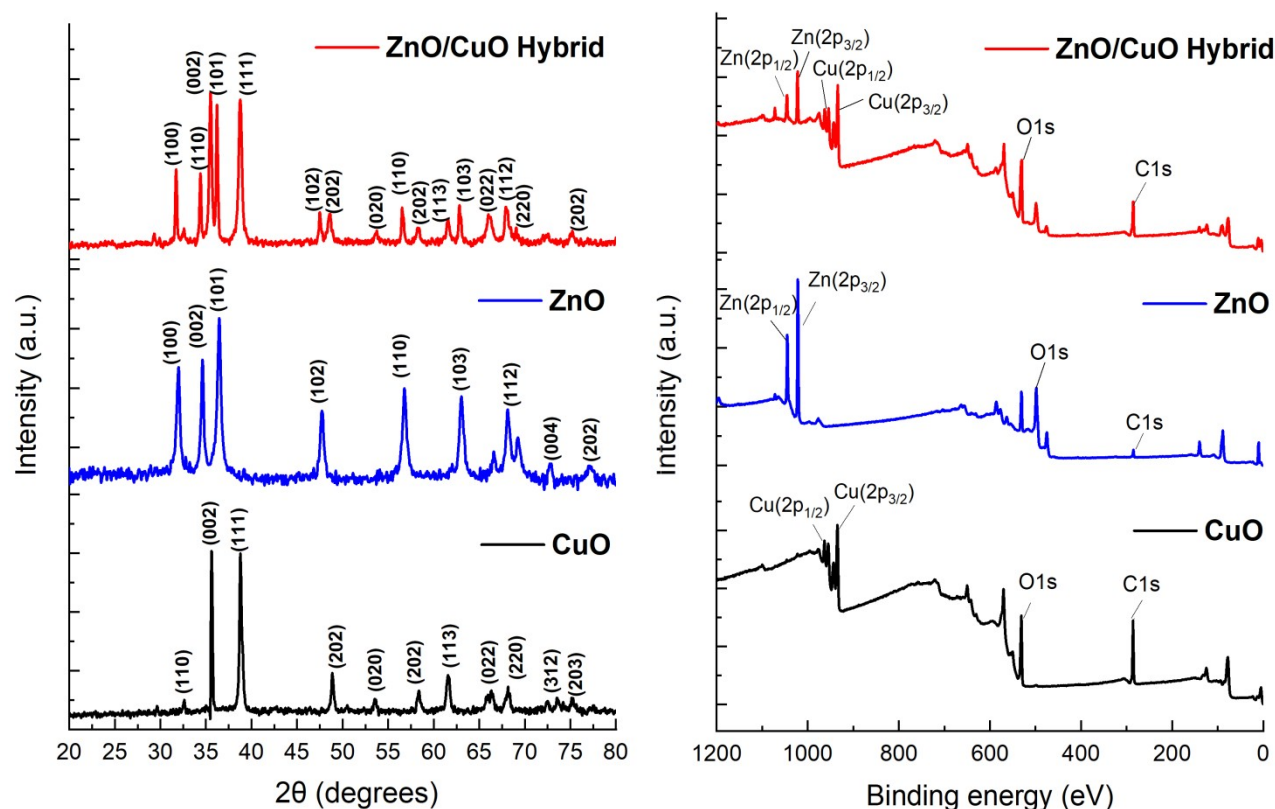


Figure 1: (a) XRD patterns, and (b) XPS spectra of ZnO, CuO and ZnO/CuO hybrid particles.

XPS analysis was studied to clarify the chemical structure of all prepared particles in terms of weight (%) values and binding energies of elements (Table 3). Figure 1 (b) shows that the XPS spectrum of

ZnO/CuO hybrid, ZnO and CuO structures and the binding energies related to Zn2p, Cu2p, O1s, and C1s peaks. When the binding energies of the ZnO/CuO hybrid structure are compared with the

pure form of ZnO structures, it is seen that the binding energy for Zn2p (1022 eV) shifts to higher binding energy (~ 0.3 eV) than for the pure form of ZnO. Furthermore, the binding energy of Cu2p (933 eV) shifted to lower energy (~ 0.7 eV) than pure CuO upon the ZnO/CuO hybrid structure formation. These shifts in binding energies can be attributed to differences in the electronegativity of metal ions. The electronegativity of Cu^{2+} is 2.0 while Zn^{2+} is 1.7 and for this reason, Cu^{2+} can easily remove electrons from Zn^{2+} . The electron shielding effect of Cu^{2+} increases and the main peak of Cu2p moves

toward lower binding energy, while Zn2p moves to the higher binding energy. For the ZnO/CuO hybrid, ZnO and CuO structures, the peaks of O1s coincide with the binding energies of 531.15, 531.04, and 531.26 eV (Table 3). According to previous studies, the peaks observed around ~ 530 eV were attributed to the lattice oxygen and the presence of O_2^- and O^- on the surface of the metal oxide structure. It has been also reported that the sensor detection performance is due to its ability to adsorb oxygen on the metal oxide surface (42).

Table 3: Binding energy (BE) and atomic weight (%) values of all metal oxide particles.

Name	ZnO/CuO Hybrid		ZnO		CuO	
	Peak BE	Weight (%)	Peak BE	Weight (%)	Peak BE	Weight (%)
Zn2p	1022.06	28.18	1021.78	74.82	-	-
Cu2p	933.85	31.05	-	-	934.59	49.57
O1s	531.15	25.20	531.04	18.62	531.26	28.91
C1s	285.16	15.57	285.29	6.56	286.04	21.52

Figure 2 (a), (b) and (c) show SEM micrographs that characterize the morphologies and microstructures of ZnO, CuO, and ZnO/CuO hybrid particles at $\times 10.0$ k magnification, respectively. According to the results, the aggregation of nanoparticles may be based on the high surface areas and energies of

ZnO and CuO particles. The formation of p-n heterojunctions along with pores and voids between p-type CuO and n-type ZnO in ZnO/CuO particles also contributes to gas sensitivity (31). As can be seen, there are much finer pores and cavities in the structure of the ZnO/CuO hybrid material.

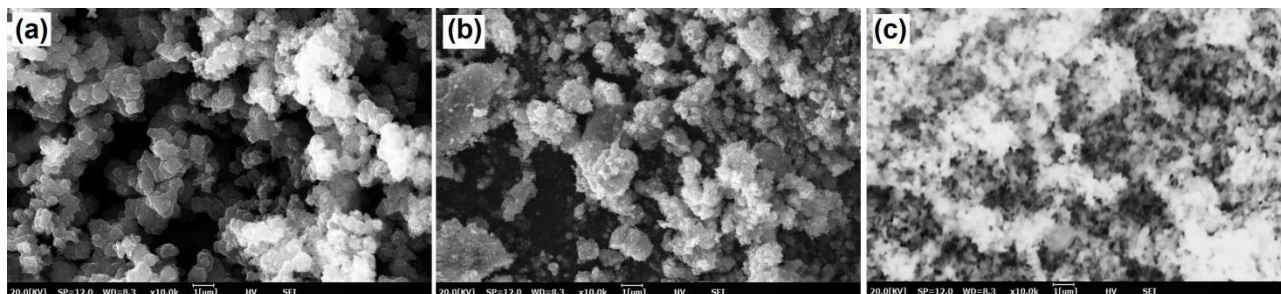


Figure 2: SEM images of (a) ZnO, (b) CuO, (c) ZnO/CuO hybrid particles at $\times 10.0$ k magnification.

Spectral behavior of H_2TPP along with metal oxide particles

Herein, we investigated the oxygen-induced spectral response of the H_2TPP along with nanoscale ZnO, CuO and ZnO/CuO hybrid particles in the poly(TMSP)-based thin films. When the H_2TPP -based sensing slides were excited at 420 nm, yielded with two emission bands at 652 and 717 nm. In all of the forms under study, the oxygen-induced emission intensities decreased which can be used as the analytical signal with the increasing quencher

amounts between the concentration ranges of 0-100% $[\text{O}_2]$. The relative signal change resulting from dynamic quenching depends on triple oxygen quenching the excited-state fluorescence of H_2TPP -based sensing composites through collisions. The following Stern-Volmer equation was used, which reveals the relationship between quencher concentration and fluorescence intensities, as it is most suitable for linearizing experimental data in the concentration interval of 0-100% $[\text{O}_2]$ (Eq. 1);

$$\frac{I_0}{I} = 1 + K_{SV}[\text{O}_2] \quad (\text{Eq. 1})$$

where I_0 and I are the fluorescence intensities in the absence and presence of quencher, respectively, KSV is the Stern–Volmer constant and $[O_2]$ is the oxygen concentration. When all other variables are kept constant, the higher the KSV, the lower concentration of quencher required to quench the luminescence (19).

The oxygen-induced fluorescence spectra of C1, C2, C3, and C4 composites were shown between Figure 3 and 6, respectively. When the porphyrin dye was used along with the metal oxide nanoparticles in the poly(TMSP) matrix in close proximity, it became extremely sensitive toward oxygen. The C1

exhibited a 70% signal drop for the 0-100% $[O_2]$ range, the C2, C3 and C4 composites yielded 80%, 75%, and 88% signal changes when exposed to the same concentration range of the oxygen, respectively. The comparative calibration plots of the utilized composites for the concentration range of 0–100% $[O_2]$ and the related equations of the calibration curves were reported in Figure 7 and Table 3, respectively. All of the H_2TPP -based sensing slides in the presence of metal oxide additives revealed linearly emission-based response in direction of decrease and exhibited good linearity and high regression coefficient (R^2) values in oxygenated conditions.

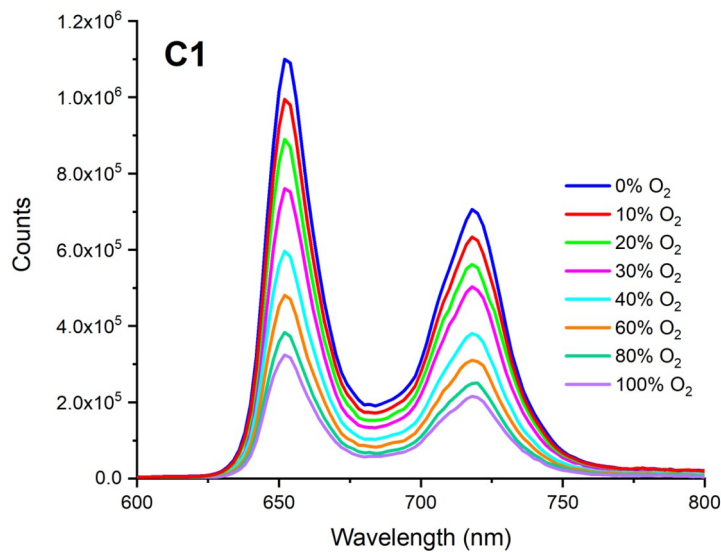


Figure 3: The oxygen induced-emission spectra of C1 in poly(TMSP) thin film for the concentration range of 0–100%.

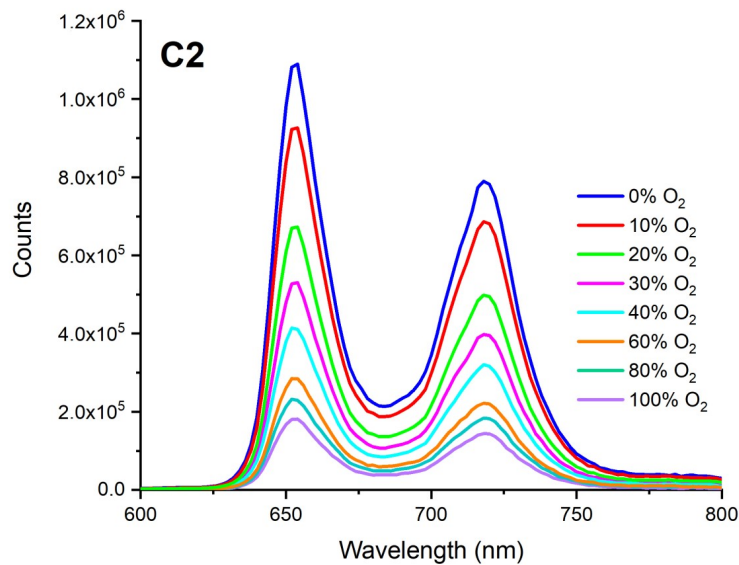


Figure 4: The oxygen induced-emission spectra of C2 in poly(TMSP) thin film for the concentration range of 0–100%.

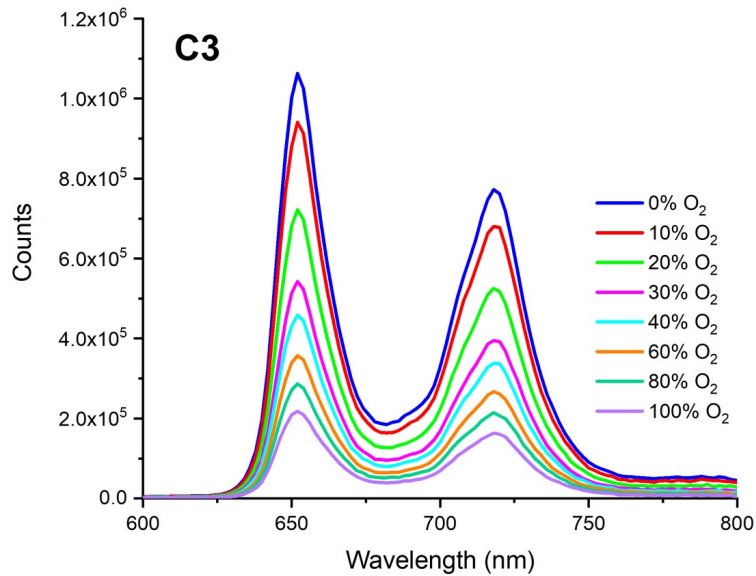


Figure 5: The oxygen induced-emission spectra of C3 in poly(TMSP) thin film for the concentration range of 0–100%.

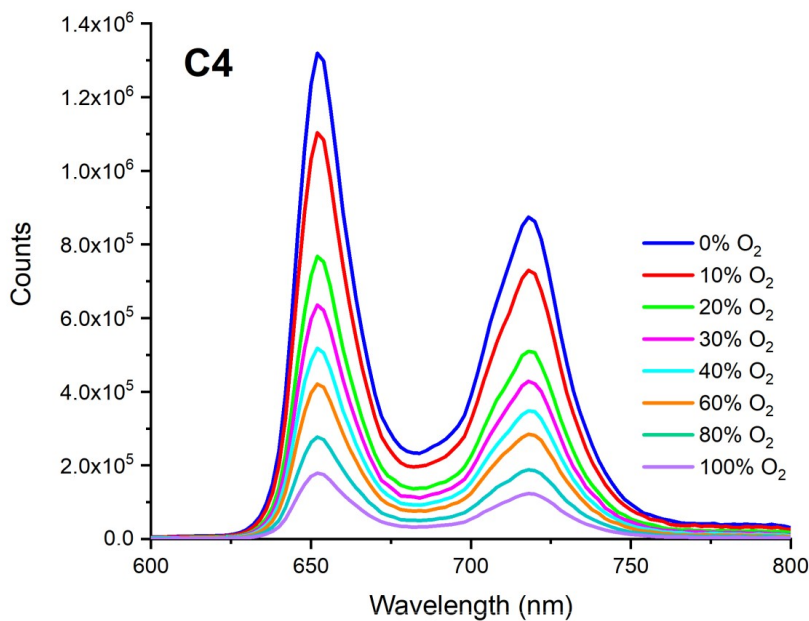


Figure 6: The oxygen induced-emission spectra of C4 in poly(TMSP) thin film for the concentration range of 0–100%.

When the emission-based signal drops of the utilized composites between 0% and 100% [O₂] were compared, C4 exhibited a superior linear response and a fairly high slope on the calibration plot relative to C1, C2, and C3; this case can be considered an indicator of the hypersensitivity of the

ZnO/CuO hybrid particle doped composite for the analyte. However, a linearized calibration plot of the C4 composite can be defined as; $y=0.0604x+1$ and the R² value of 0.9817 for the concentration range of 0-100% [O₂].

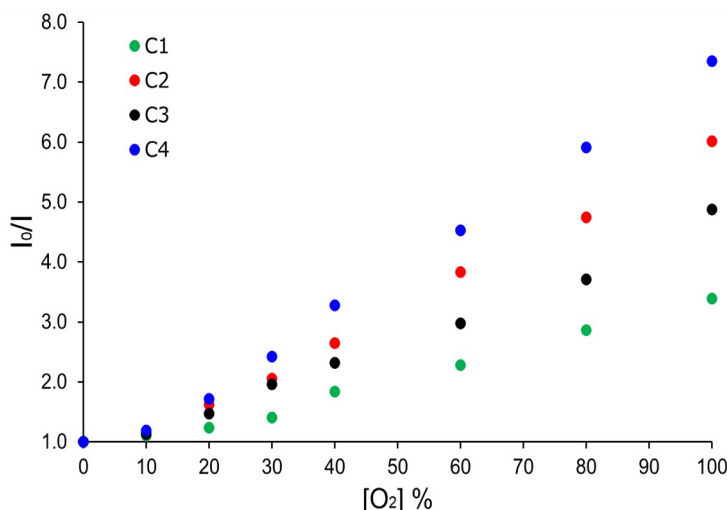


Figure 7: The comparative calibration plots of the C1, C2, C3, and C4 composites for the concentration range of 0-100% [O₂].

Table 4 reveals the equations of the calibration curves, the regression coefficients, the Stern-Volmer constants (K_{sv}), the relative signal changes (I_0/I_{100}) and the limit of detection (LOD) values of the utilized composites. The I_0/I_{100} ratio has been accepted as a display of indicator sensitivity where I_0 and I_{100} are the signal intensities of the indicator dye in the lack of and the maximum concentration levels of quencher, respectively. Nevertheless, the researches to improve the I_0/I_{100} parameter of the H₂TPP are still in progress. Herein, the utilization of the ZnO, CuO and ZnO/CuO hybrid powders along with the H₂TPP in the silicon matrix resulted in enhanced sensitivity with respect to the former literature (18,19). The I_0/I_{100} values were found to be 3.39, 6.02, 4.88, and 7.35 for the C1, C2, C3, and C4, respectively. The Stern-Volmer (K_{sv}) values, which quantifies the quenching efficiency of the sensor, were found in the range of 2.25×10^{-2} –

6.04×10^{-2} for all of the thin film-based composites. As a result, it can be concluded that C4 exhibits better oxygen gas sensitivity as it shows higher relative signal change and KSV values compared to other cocktails. This result makes the C4 composite an encouraging sensor slide for developing a luminescence-based oxygen detecting device. Also, the limit of detection (LOD) value is calculated using both the slope of the extinction plot in the calibration graph and the resolution of the spectroscopic instrument and calculated by dividing the $0.003/\text{slope}$ at a signal-to-noise ratio of 3.0. Considering the fully-nitrogen gas moiety as the blank, the LOD values for the C1, C2, C3, and C4 were found to be 1.25×10^{-2} p[O₂]% (1.66×10^{-1} mg/L), 2.21×10^{-2} p[O₂]% (2.94×10^{-1} mg/L), 1.89×10^{-2} p[O₂]% (2.51×10^{-1} mg/L), and 2.84×10^{-2} p[O₂]% (3.78×10^{-1} mg/L), respectively (Table 4).

Table 4: Optical properties and O₂ sensitivity of H₂TPP dye included sensing agents.

Cocktail name	Equation (Conc.range of 0–100% [O ₂])	Stern-Volmer constant K_{sv}	Regression coefficient R^2	I_0/I_{100}	LOD (p[O ₂]%)	LOD (mg/L)
C1	$y=0.0225x + 1$	2.25×10^{-2}	0.9702	3.39	1.25×10^{-2}	1.66×10^{-1}
C2	$y=0.0471x + 1$	4.71×10^{-2}	0.9798	6.02	2.21×10^{-2}	2.94×10^{-1}
C3	$y=0.0355x + 1$	3.55×10^{-2}	0.9785	4.88	1.89×10^{-2}	2.51×10^{-1}
C4	$y=0.0604x + 1$	6.04×10^{-2}	0.9817	7.35	2.84×10^{-2}	3.78×10^{-1}

In this study, we independently measured the absorption and the emission bands of the heterostructures of H₂TPP and all utilized additives to clarify the reasons behind the increase of oxygen-induced sensitivity. The normalized intensity-based spectra of ZnO, CuO and ZnO/CuO hybrid particles were individually shown in Figure 8 (a), (b) and (c), superimposed with the intensity-based spectrum of

the H₂TPP dye. All the utilized powders embedded in the poly(TMSP) thin-film were excited at their own excitation wavelength. Both ZnO, CuO and ZnO/CuO hybrid additives excited in a wide range wavelength, which covers the excitation band of H₂TPP, between 300 and 450 nm and emitted in broadband of approximately 400 to 720 nm.

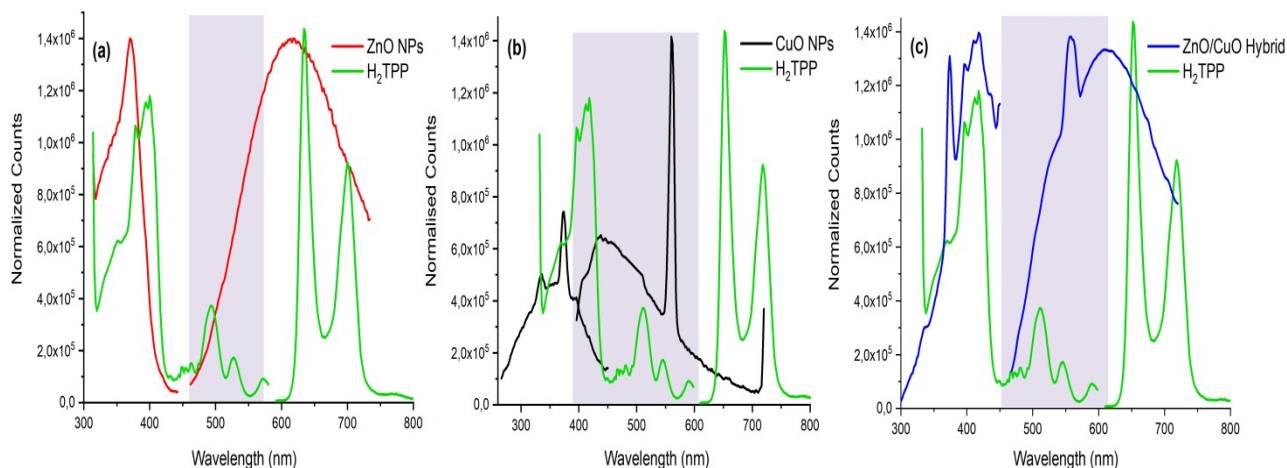


Figure 8: The excitation and emission spectra of the poly(TMSP) embedded H₂TPP, (a) ZnO, (b) CuO and (c) ZnO/CuO hybrid, individually.

The gas sensing performances of ZnO and CuO semiconductor materials are related to the oxygen adsorption and electron transfer process. The presence of active pores, void spaces and oxygen vacancies, which act as active centers for the adsorption of oxygen molecules, enable the semiconductor oxides to exhibit high gas sensing capacity. Also, the free electrons on the surface of ZnO and CuO semiconductors result in the enhancement of gas sensitivity by adsorbing a large number of oxygen species from the air. When CuO and ZnO materials have interacted, electrons can migrate from n-type ZnO to p-type CuO as a result of a strong effect between both semiconductor materials and hence more free electrons are available in this system. The more enhanced oxygen response of ZnO/CuO hybrid heterostructures is due to larger p-n junction depletion regions, larger surface area, and more oxygen adsorption at the surface, resulting from the formation of p-n heterojunctions between p-type CuO and n-type ZnO (31).

The enhancement in the oxygen sensitivity of H₂TPP in the presence of the metal oxide particles may be attributed to the strong excitation-emission abilities of the metal oxides, which act as a light-harvesting agent, and the energy transfer between the metal oxide particles and the dye. According to Figure 8 (a), (b) and (c), the emission bands of all utilized metal oxide additives partially overlaps with the absorption band of the H₂TPP, which makes interaction and an energy transfer from the metal oxide particles (donor) to the porphyrin dye (acceptor), possible. The strong absorption and the broadband emission of ZnO and CuO semiconductor materials are associated with a charge transfer from the 2p levels of the O₂ at the valence band (VB) to the 3d orbitals of the metal ions lying in the conduction band (CB). However, the coexistence of the CuO and ZnO nanocrystals in the hybrid

structure resulted in an unexpected enhancement in the oxygen sensitivity of the H₂TPP. The broad emission band (from 450 to 720 nm) of the ZnO/CuO hybrid crystals may be attributed to the direct electron transitions between the CB and the VB or the transition of the electrons from the defect orbitals to the CB or VB. However, the emission performance corresponds to the green-yellow region of the spectrum of ZnO/CuO hybrid particles originating from metal ions and cavities of oxygen, interstitial metal ions, electronic transitions between interstitial metal ions, and oxygen antisite increases the oxygen detection abilities of H₂TPP (25,42,43).

Decay Time Measurements

In this work, the luminescence decay time kinetics of all the used sensing slides were measured under oxygenated and deoxygenated atmosphere (Figure 9). When excited at 418 nm, the H₂TPP-based composites exhibited tri-exponential and bi-exponential decays in oxygen-free and fully-oxygenated conditions, respectively. Short and long decay time components and their distribution statistics for all sensing slides were shown in Table 5. The observed multi-exponential features in decay kinetics may be ascribed to as the structural features of the fluorophore composites and the hassle of the accessibility of the quencher. In deoxygenated moieties, the decay-time values of the undoped- and the additive doped-H₂TPP composites varied between 2.40 and 2.47 μ s for the short lifetime components and between 100.86 and 109.32 μ s for the long one. When exposed to oxygen, the shorter decay time components between 2.98 and 1.06 μ s and the longer lifetime components between 11.54 and 9.88 μ s were observed for all of the sensing slides. When exposed to oxygen, the longer lifetime component got lost (around \sim 100.00 μ s) and the average decay times showed a decrease of 20, 30, 25, and 40% for C1, C2, C3, and C4, respectively.

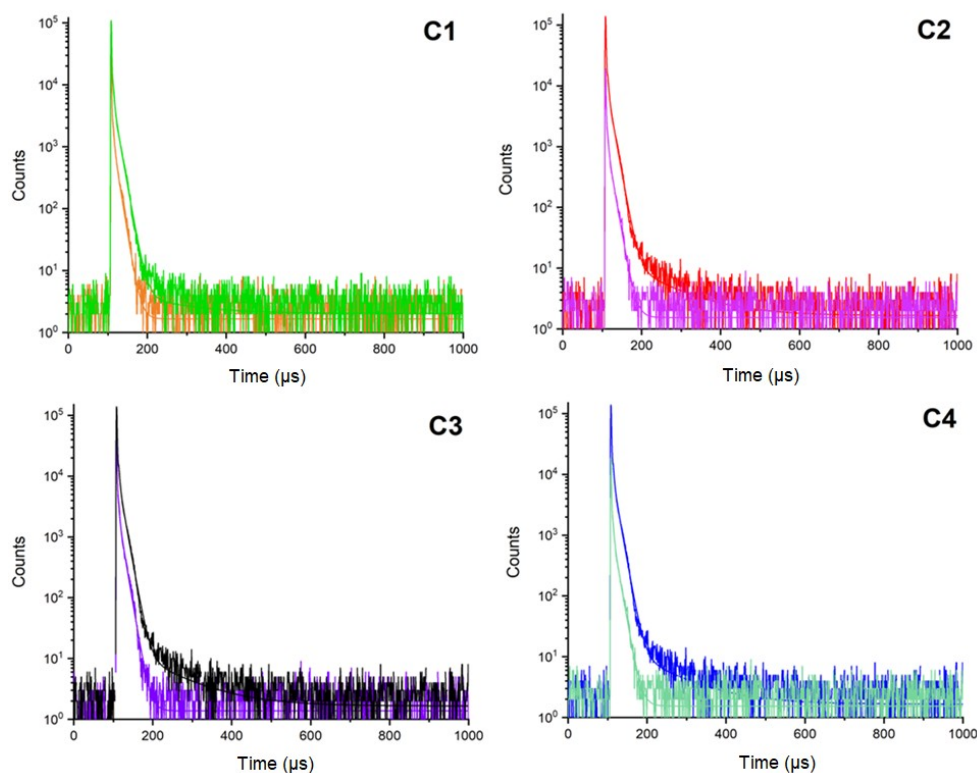


Figure 9: The decay kinetics of C1, C2, C3, and C4 under exposure to under fully-nitrogen and fully-oxygen atmosphere.

In fully oxygenated moieties, the increased signal decrease rates observed in both the emission-based intensity and the decay kinetics can be explained by the existence of metal oxides providing better adsorption properties of oxygen. In such metal oxide particles, the adsorbed oxygen gas diffuses to the inside or subsurface layer of the oxygen-induced luminescent dye. Also, the adsorbed or diffused gas in metal oxide semiconductors creates potential barriers between the oxide grains, which reduction in electrical conductivity. This charge mobility in metal oxides, which affects luminescence and conductivity decreases in decay time values (44).

Reversibility and Stability of the H₂TPP-based Composites

Response-regeneration time and stability are significant properties of optical sensor performance. The intensity-based kinetic response of the H₂TPP-based composites along with the ZnO, CuO and ZnO/CuO hybrid additives were individually investigated and evaluated to time under fully-

nitrogen and fully-oxygen atmosphere. The reversible signal cycles for kinetic measurements were measured along 1000 s. After exposure to fully-oxygenated atmosphere, the response times of C1, C2, C3, and C4 were measured as 16, 12, 14, and 10 s, and the regeneration times for the reverse direction were determined as 34, 24, 28, and 20 s, respectively (Figure 10). Considering these results, when compared to the other H₂TPP based-sensing slides, the C4 showed better response-regeneration time and repeatability results over multiple detection cycles under conditions of constantly changing gas concentrations between 0% and 100% O₂. Also, no significant decrease was monitored in the oxygen-induced intensities and decay kinetics of the sensing agents when stored at the ambient air of the laboratory conditions ($20 \pm 1^\circ\text{C}$) in the dark for 6 months. The utilized sensing slides had lost their original intensity-based signal values less than 3%, but they still had the potential for O₂ gas measurements.

Table 5: Decay kinetics of C1, C2, C3, and C4 embedded in the poly(TMSP)-based thin films.

Sample	τ_0 (0% O ₂)	Decay Time (μ s)	Std. Dev. (μ s)	Rel. (%)	τ_0 (100% O ₂)	Decay Time (μ s)	Std. Dev. (μ s)	Rel. (%)
C1	τ_2	2.47	0.07	21.48	τ_2	2.98	0.16	33.46
	τ_3	11.73	0.08	77.27	τ_3	11.54	0.20	66.54
	τ_4	107.98	1.08	1.25	τ_4	-	-	-
	T_{avr}		10.95 μ s		T_{avr}		8.67 μ s	
C2	τ_2	2.45	0.06	22.43	τ_2	2.19	0.14	35.38
	τ_3	11.96	0.07	76.60	τ_3	10.44	0.19	64.62
	τ_4	109.32	1.22	0.97	τ_4	-	-	-
	T_{avr}		10.77 μ s		T_{avr}		7.52 μ s	
C3	τ_1	2.46	0.07	21.41	τ_1	2.82	0.09	33.98
	τ_2	11.72	0.08	77.34	τ_2	11.19	0.12	66.02
	τ_3	107.12	1.06	1.26	τ_3	-	-	-
	T_{avr}		10.94 μ s		T_{avr}		8.34 μ s	
C4	τ_1	2.40	0.06	19.91	τ_1	1.06	0.01	38.77
	τ_2	11.69	0.06	79.10	τ_2	9.88	0.06	61.23
	τ_3	100.86	0.09	0.99	τ_3	-	-	-
	T_{avr}		10.72 μ s		T_{avr}		6.46 μ s	

CONCLUSION

In this work, we reported the effect of the gas adsorption properties of metal oxide additives on the oxygen sensitivity of the H₂TPP via the enhancement in the emission spectra. The XRD, XPS, SEM, and PL spectroscopic techniques were used for the characterization of the synthesized ZnO, CuO and ZnO/CuO hybrid particles. The oxygen-sensitivities of the H₂TPP-based composites and the interactions between the porphyrin dye and the metal oxide additives were tested with fluorescence-based measurements and decay time kinetics. The relative signal changes (I_0/I_{100}) of 3.39,

6.02, 4.88, and 7.35 were reported for the poly(TMSP) embedded C1, C2, C3, and C4, respectively. The most sensitive detection slide, C4, showed a linear response for the concentration range of 0-100% [O₂] with an R² value of 0.9817 and a high slope on the calibration graph. The enhancement in the oxygen-induced sensitivity of H₂TPP should be attributed not only to the excitation-emission abilities of the ZnO/CuO hybrid additives but also to the free electrons formed during the generation of heterojunction between ZnO and CuO in the synthesis of the ZnO/CuO structure, which facilitates the adsorption of O₂ molecules on the surface.

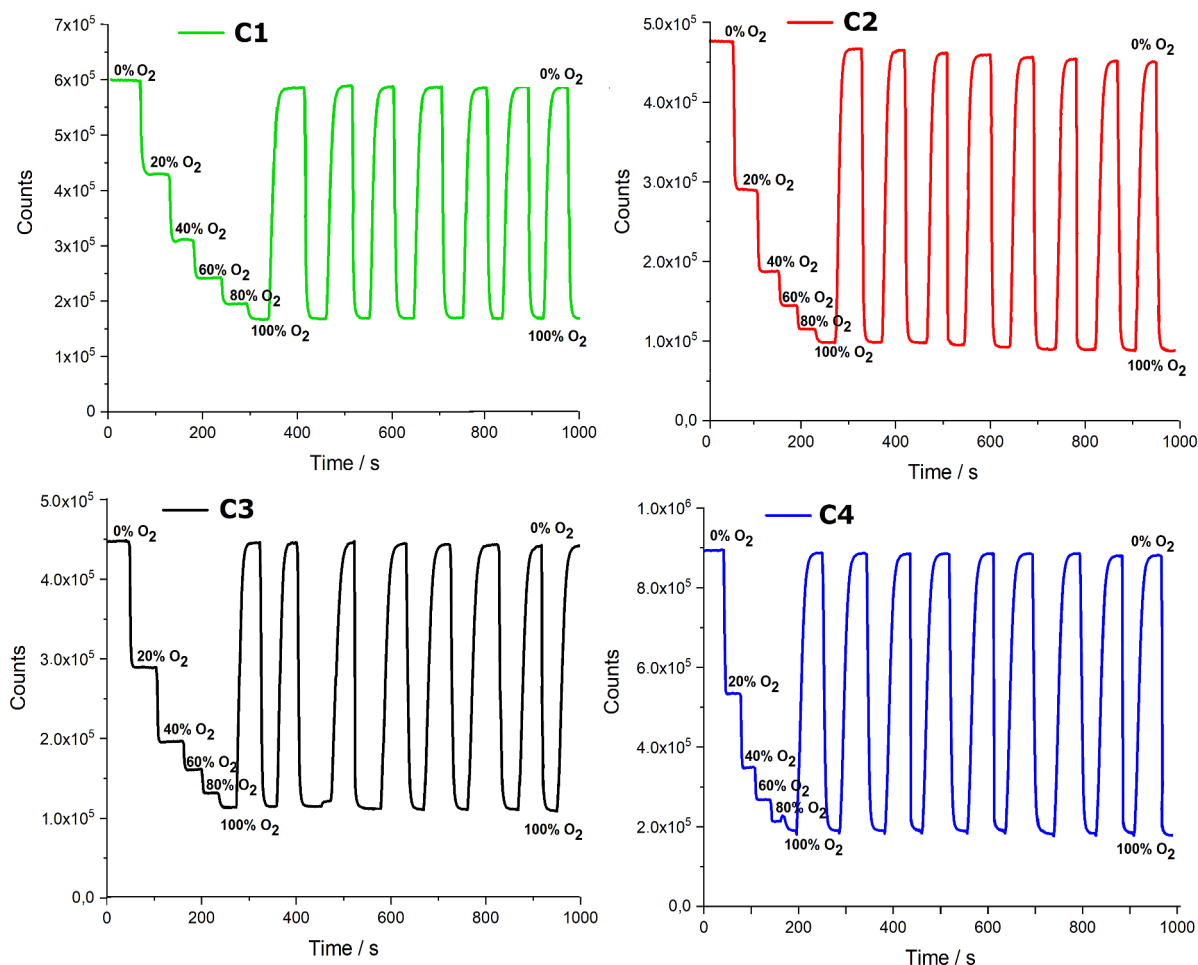


Figure 10: Intensity-based kinetic response of C1, C2, C3, and C4 composites between the oxygen concentrations of 0% and 100%.

ACKNOWLEDGMENT

Financing for steady-state and decay time measurements of meso-tetraphenylporphyrin dye was obtained from Dokuz Eylul University Scientific Research Funds (Project no: 2018.KB.FEN.039). Also, XRD, XPS, and PL measurements were performed in the Center for Fabrication and Applications of Electronic Materials (EMUM). I would like to thank them all.

CONFLICT OF INTEREST

The author declares that there are no conflicts of interest.

REFERENCES

1. Passard G, Dogutan DK, Qiu M, Costentin C, Nocera DG. Oxygen reduction reaction promoted by manganese porphyrins. *ACS Catal.* 2018;8(9):8671–9. [<DOI>](#).
2. Xu Y, Yang D, Huo S, Ren J, Gao N, Chen Z, et al. Carbon dots and ruthenium doped oxygen sensitive nanofibrous membranes for monitoring the respiration of agricultural products. *Polym Test.* 2021;93:106957. [<DOI>](#).
3. Canaparo R, Foglietta F, Limongi T, Serpe L. Biomedical applications of reactive oxygen species generation by metal nanoparticles. *Materials (Basel).* 2021;14(1):53. [<DOI>](#).
4. Wang G, Chen H. Oxygen consumption for the combustion of sewage sludge: a potential environmental parameter determined by an electrochemical YSZ oxygen sensor. *Int J Environ Anal Chem.* 2020;1–10. [<DOI>](#).
5. Kuang C, Wang S, Luo M, Cai J, Zhao J. Investigation of CuO-based oxygen carriers modified by three different ores in chemical looping combustion with solid fuels. *Renew Energy.* 2020;154:937–48. [<DOI>](#).
6. Ongun MZ, Sahin M, Akbal T, Avsar N, Karakas H, Ertekin K, et al. Synthesis, characterization and oxygen sensitivity of cyclophosphazene equipped-iridium (III) complexes. *Spectrochim Acta Part A Mol Biomol Spectrosc.* 2020;239:118490. [<DOI>](#).
7. Monash A, Marciano D, Fass R, Dvash Y, Rosen O. Phosphorescent palladium-tetrabenzoporphyrin indicators for immunosensing of small molecules with a novel optical device. *Talanta.* 2021;224:121927. [<DOI>](#).

8. Xing Y, Wang L, Liu C, Jin X. Effects of fluorine and phenyl substituents on oxygen sensitivity and photostability of cyclometalated platinum (II) complexes. *Sensors Actuators B Chem.* 2020;304:127378. [<DOI>](#).
9. Ge C, Zhu J, Ouyang A, Lu N, Wang Y, Zhang Q, et al. Near-infrared phosphorescent terpyridine osmium (II) photosensitizer complexes for photodynamic and photooxidation therapy. *Inorg Chem Front.* 2020;7(20):4020-7. [<DOI>](#).
10. Bolognesi M, Moschetto S, Trapani M, Prescimone F, Ferroni C, Manca G, et al. Noncovalent functionalization of 2D black phosphorus with fluorescent boronic derivatives of pyrene for probing and modulating the interaction with molecular oxygen. *ACS Appl Mater Interfaces.* 2019;11(25):22637-47. [<DOI>](#).
11. Ongun MZ, Topal SZ, Yel Z, Ertekin K, Önal E, Hirel C. Improvement of the O₂ detection: Substituent's effect on Pd (II) meso-tetraphenylporphyrin probes. *Sensors Actuators B Chem.* 2019;288:316-24. [<DOI>](#).
12. Önal E, Ay Z, Yel Z, Ertekin K, Gürek AG, Topal SZ, et al. Design of oxygen sensing nanomaterial: synthesis, encapsulation of phenylacetylide substituted Pd (II) and Pt (II) meso-tetraphenylporphyrins into poly (1-trimethylsilyl-1-propyne) nanofibers and influence of silver nanoparticles. *RSC Adv.* 2016;6(12):9967-77. DOI: [<DOI>](#).
13. Chu C-S, Chuang C-Y. Ratiometric optical fiber dissolved oxygen sensor based on metalloporphyrin and CdSe quantum dots embedded in sol-gel matrix. *J Lumin.* 2015;167:114-9. [<DOI>](#).
14. Borisov SM, Lehner P, Klimant I. Novel optical trace oxygen sensors based on platinum (II) and palladium (II) complexes with 5, 10, 15, 20-meso-tetrakis-(2, 3, 4, 5, 6-pentafluorophenyl)-porphyrin covalently immobilized on silica-gel particles. *Anal Chim Acta.* 2011;690(1):108-15. [<DOI>](#).
15. Oige K, Avarmaa T, Suisalu A, Jaaniso R. Effect of long-term aging on oxygen sensitivity of luminescent Pd-tetraphenylporphyrin/PMMA films. *Sensors Actuators B Chem.* 2005;106(1):424-30. [<DOI>](#).
16. Mueller BJ, Burger T, Borisov SM, Klimant I. High performance optical trace oxygen sensors based on NIR-emitting benzoporphyrins covalently coupled to silicone matrixes. *Sensors Actuators B Chem.* 2015;216:527-34. [<DOI>](#).
17. Amao Y, Asai K, Okura I. Oxygen sensing based on lifetime of photoexcited triplet state of platinum porphyrin-polystyrene film using time-resolved spectroscopy. *J Porphyr Phthalocyanines.* 2000;4(3):292-9. [<DOI>](#).
18. Topal SZ, Ongun MZ, Önal E, Ertekin K, Hirel C. Hyperporphyrin effect on oxygen sensitivity of free meso-tetraphenylporphyrins. *Dye Pigment.* 2017;144:102-9. [<DOI>](#).
19. Topal SZ, Önal E, Ertekin K, Oter O, Gürek AG, Hirel C. Significant sensitivity and stability enhancement of tetraphenylporphyrin-based optical oxygen sensing material in presence of perfluorochemicals. *J Porphyr Phthalocyanines.* 2013;17(06n07):431-9. [<DOI>](#).
20. Potyrailo RA, Hieftje GM. Oxygen detection by fluorescence quenching of tetraphenylporphyrin immobilized in the original cladding of an optical fiber. *Anal Chim Acta.* 1998;370(1):1-8. [<DOI>](#).
21. Arafat MM, Dinan B, Akbar SA, Haseeb A. Gas sensors based on one dimensional nanostructured metal-oxides: a review. *Sensors.* 2012;12(6):7207-58. [<DOI>](#).
22. Wang JX, Sun XW, Yang Y, Kyaw KKA, Huang XY, Yin JZ, et al. Free-standing ZnO-CuO composite nanowire array films and their gas sensing properties. *Nanotechnology.* 2011;22(32):325704. [<DOI>](#).
23. Jiang T, Du B, Zhang H, Yu D, Sun L, Zhao G, et al. High-performance photoluminescence-based oxygen sensing with Pr-modified ZnO nanofibers. *Appl Surf Sci.* 2019;483:922-8. [<DOI>](#).
24. Qu X, Yang R, Tong F, Zhao Y, Wang M-H. Hierarchical ZnO microstructures decorated with Au nanoparticles for enhanced gas sensing and photocatalytic properties. *Powder Technol.* 2018;330:259-65. [<DOI>](#).
25. Ongun MZ. Tuning CO₂ sensitivity of HPTS by ZnO and ZnO@ Ag nanoparticles. *J Photochem Photobiol A Chem.* 2020;400:112664. [<DOI>](#).
26. Yin X-T, Dastan D, Wu F-Y, Li J. Facile synthesis of SnO₂/LaFeO₃- XNX composite: photocatalytic activity and gas sensing performance. *Nanomaterials.* 2019;9(8):1163. [<DOI>](#).
27. Paliwal A, Sharma A, Tomar M, Gupta V. Carbon monoxide (CO) optical gas sensor based on ZnO thin films. *Sensors Actuators B Chem.* 2017;250:679-85. [<DOI>](#).
28. Castellero P, Roales J, Lopes-Costa T, Sánchez-Valencia JR, Barranco A, González-Elipe AR, et al. Optical gas sensing of ammonia and amines based on protonated porphyrin/TiO₂ composite thin films. *Sensors.* 2017;17(1):24. [<DOI>](#).
29. Chethana DM, Thanuja TC, Mahesh HM, Kiruba MS, Jose AS, Barshilia HC, et al. Synthesis, structural, magnetic and NO₂ gas sensing property of CuO nanoparticles. *Ceram Int.* 2021;47(7):10381-7. [<DOI>](#).
30. Priya AK, Sunny A, Karthikeyan B, Sastikumar D. Optical, spectroscopic and fiber optic gas sensing of potassium doped α -Fe₂O₃ nanostructures. *Opt Fiber Technol.* 2020;58:102304. [<DOI>](#).
31. Mariammal RN, Ramachandran K. Study on gas sensing mechanism in p-CuO/n-ZnO heterojunction sensor. *Mater Res Bull.* 2018;100:420-8. [<DOI>](#).
32. Sanchez-Valencia JR, Alcaire M, Romero-Gómez P, Macias-Montero M, Aparicio FJ, Borrás A, et al. Oxygen optical sensing in gas and liquids with nanostructured ZnO thin films based on exciton emission detection. *J Phys Chem C.* 2014;118(18):9852-9. [<DOI>](#).
33. Jiang Z, Yu X, Zhai S, Hao Y. Ratiometric dissolved oxygen sensors based on ruthenium complex doped with silver nanoparticles. *Sensors.* 2017;17(3):548. [<DOI>](#).
34. Ozturk O, Oter O, Yildirim S, Subasi E, Ertekin K, Celik E, et al. Tuning oxygen sensitivity of ruthenium

complex exploiting silver nanoparticles. *J Lumin.* 2014;155:191–7. <DOI>.

35. Ongun MZ. Development of Highly Sensitive Metal-Free Tetraphenylporphyrin-Based Optical Oxygen Sensing Materials along with ILs and AgNPs. *Celal Bayar Univ J Sci.* 2019;15(1):131–8. DOI: <DOI>.

36. Oguzlar S. Development of highly sensitive [Ru (bpy) 3] 2+-Based optical oxygen sensing thin films in the presence with Fe3O4 and Fe3O4@ Ag NPs. *Opt Mater (Amst).* 2020;101:109772. <DOI>.

37. Yildirim B, Keskin OY, Oguzlar S, Birlik I, Azem FA, Ertekin K. Manipulation of brightness and decay kinetics of LuAG: Ce3+ and YAG: Ce3+ by simple metal oxides in polymeric matrices. *Opt Laser Technol.* 2021;142:107226. <DOI>.

38. Yang C, Cao X, Wang S, Zhang L, Xiao F, Su X, et al. Complex-directed hybridization of CuO/ZnO nanostructures and their gas sensing and photocatalytic properties. *Ceram Int.* 2015;41(1):1749–56. <DOI>.

39. Ongun MZ, Oter O, Sabancı G, Ertekin K, Celik E. Enhanced stability of ruthenium complex in ionic liquid doped electrospun fibers. *Sensors Actuators B Chem.* 2013;183:11–9. <DOI>.

40. Acedo-Mendoza AG, Infantes-Molina A, Vargas-Hernández D, Chávez-Sánchez CA, Rodríguez-Castellón E, Tánori-Córdova JC. Photodegradation of methylene blue and methyl orange with CuO supported on ZnO photocatalysts: The effect of copper loading and reaction temperature. *Mater Sci Semicond Process.* 2020;119:105257. <DOI>.

41. Zhu D, Wang L, Yu W, Xie H. Intriguingly high thermal conductivity increment for CuO nanowires contained nanofluids with low viscosity. *Sci Rep.* 2018;8(1):1–12. DOI: <DOI>.

42. Wang X, Li S, Xie L, Li X, Lin D, Zhu Z. Low-temperature and highly sensitivity H2S gas sensor based on ZnO/CuO composite derived from bimetal metal-organic frameworks. *Ceram Int.* 2020;46(10):15858–66. <DOI>.

43. Oguzlar S, Ongun MZ, Ertekin K. Investigation of light induced interactions between ZnO nano-particles and red emitting phosphor blends of Eu2+/Dy3+ doped strontium aluminate and Eu2+ doped Ca- α -Sialon. *J Lumin.* 2021;118236. <DOI>.

44. Aydin I, Ertekin K, Demirci S, Gultekin S, Celik E. Sol-gel synthesized Sr4Al14O25: Eu2+/Dy3+ blue-green phosphorous as oxygen sensing materials. *Opt Mater (Amst).* 2016;62:285–96. <DOI>.

